J Mater Sci (2015) 50:5145–5156
DOI 10.1007/s10853-015-9047-4

Synthesis of TiO_2-doped mesoporous nanobioactive glass particles and their cytocompatibility against osteoblast cell line

V. Rajendran[1] · M. Prabhu[1] · R. Suriyaprabha[1]

Received: 3 December 2014 / Accepted: 21 April 2015 / Published online: 8 May 2015

Abstract To obtain medically important mesoporous biomaterial, we prepared titanium-doped nanobioactive glass (NBG) particles $55SiO_2$–$(36 - x)$ CaO–$9P_2O_5$–$xTiO_2$ ($x = 0$, 1, 2, and 3 mol%) were prepared by simple sol–gel method. The physicochemical properties of the prepared nanocomposites were analyzed using different characterization techniques. The developed mesoporous nanocomposites showed amorphous nature with globular morphology, with a particle size of approximately 50 nm. The specific surface area of glass nanocomposites doped with TiO_2 at different concentrations, namely SCPT0 (0 %), SCPT1 (1 %), SCPT2 (2 %), and SCPT3 (3 %) samples, was 129, 186, 105, and 129 $m^2\ g^{-1}$, respectively. In addition, the average pore diameter of the glass series was 33, 18, 27, and 25 nm. The in vitro bioactivity of hydroxyapatite layer formation was confirmed using simulated body fluid. Further, antibacterial property of mesoporous nanocomposites was investigated against *Escherichia coli* and *Staphylococcus aureus*. The diameter of the inhibition zone of TiO_2-doped nanocomposites against *E. coli* was found to be 16, 18, and 20 mm. No significant inhibition was found for Ti-free samples against *E. coli* and *S. aureus*. The cytotoxicity assay revealed that the prepared NBG particles doped with 1 % TiO_2 were nontoxic and showed better cell viability in osteoblast cell line (MG-63) at a concentration of 125 μg ml^{-1}. Therefore, the addition of biomimic metal oxide dopant such as TiO_2 in NBGs is an effective approach to develop a highly biocompatible material for bone implant applications.

Introduction

Calcium phosphate-based bioactive and bioresorbable glass particles are known for their enhanced biological properties for scaffold preparation and tissue-engineering applications [1]. Particularly, nanobioactive glasses (NBGs) show outstanding physicochemical properties and enhanced biological behaviors [2]. So far many silica- and phosphate-based glass series have been studied to explore the elusive role of different compositions for biomedical applications [3, 4]. Among them, silicate-based series (SiO_2–CaO–P_2O_5) is found better for molecular interaction and hydroxyapatite (HAp) layer formation because silicon is a good glass-networking element. Silicon has low dissolution rate and low bioactivity [3]. However, NBG biocompatibility and antimicrobial properties, along with interaction of osteocytes, principally depend on additives and the ratio of bioactive glass compositions.

The optimization of NBGs doped with magnesium and silver for better in vitro bioactivity and antimicrobial properties is well studied in our previous investigations [2, 5]. The results of these studies show that MgO does not have a significant antimicrobial property even though it has better cytocompatibility against human gastric adenocarcinoma cell line. Similarly, silver is found to be toxic to

✉ V. Rajendran
veerajendran@gmail.com

M. Prabhu
prabhubpt16@gmail.com

R. Suriyaprabha
rsuriyaprabha@gmail.com

[1] Centre for Nano Science and Technology, K. S. Rangasamy College of Technology, Tiruchengode 637215, Tamil Nadu, India

human cells beyond its optimal dosage regime (>3 %) for biomedical application despite the fact that it possesses low dissolution rate. Therefore, it is essential to find out an appropriate NBG composite, which is porous and biomimic in nature, to facilitate easy cell fluid flow and bone ingrowth for tissue-engineering applications. Hence, making the choice of an efficient and appropriate dopant for calcium phosphate-based NBG particles for implant coating is currently a demanding task.

Titanium dioxide (TiO_2)-doped sodium-free calcium phosphate-based glass thin films doped with transition metal ions and TiO_2 with chitosan are a promising biomaterials as they have excellent physicochemical properties and exhibit better bioactivity and biocompatibility behavior as well as osteoblast differentiation [6–10]. Addition of TiO_2 into NBG system induces bone regeneration through HAp layer formation. Further, in an appropriate stoichiometric ratio, it enhances the in vitro bioactivity and mechanical property, thereby controlling the solubility and providing a stable surface for cell attachment [11, 12]. The development of sodium-based titanium phosphate NBG microspheres reveals good biocompatibility and in vitro bioactivity for bone tissue engineering [13, 14]. SiO_2–CaO–P_2O_5 added with TiO_2 glass ceramics is considered to be safe and non-toxic for human tissue [15, 16]. Moreover, TiO_2-added soda-lime phosphate bioglasses show interesting results during HAp crystallization [15]. In addition, Chen et al. [17] successfully synthesized polydimethylsiloxane (PDMS)-modified CaO–SiO_2–TiO_2 hybrids by sol–gel process for rapid formation of HAp [17].

Titanium dioxide (TiO_2) has been extensively studied as a powerful antibacterial substance as TiO_2 shows strong oxidizing power through the generation of hydroxyl radicals (OH^-) and superoxide anions (O_2^-) under irradiation with UV light [18, 19]. Synthesis of bioactive glass nanoparticles by sol–gel method is easy and cost-effective when compared with that by melt quenching owing to its unique advantages such as low processing temperature, higher purity, better homogeneity, mesoporosity, and increased surface area [3].

Therefore, incorporation of TiO_2 as a potent nucleating agent into NBG systems renders good porosity with better bioactivity and biocompatibility. The objective of this study was to synthesize a series of mesoporous NBG particles $55SiO_2$–$(36 - x)$ CaO–$9P_2O_5$–$xTiO_2$ ($x = 0$, 1, 2, and 3 mol%) and to characterize the physicochemical nature of the prepared nanocomposites. In addition, the in vitro bioactivity, antimicrobial activity, and cytotoxicity of the prepared NBG particles were ascertained using simulated body fluid (SBF), *Staphylococcus aureus*, *Escherichia coli*, and human osteoblast cell lines (MG-63) for dental restoration and implant applications.

Materials and methods

Materials

Tetraethyl orthosilicate (TEOS; 99 %; Sigma-Aldrich), triethylphosphate (TEP; 99.5 %; HiMedia, Mumbai), calcium nitrate ($Ca(NO_3)_2{\cdot}4H_2O$; 98 %; Merck), titanium isopropoxide (99 %; Merck), 2 N nitric acid (HNO_3; 69 %; Merck), ethanol, 1M ammonia (25 %; Merck), and ultrapure water (arium 611UF; Sartorius AG) were used without any further purification for the preparation of mesoporous NBG particles.

Sol–gel synthesis of mesoporous nanobioactive glass particles

Mesoporous NBG particles ($55\ \%SiO_2$–$(36 - x)\%CaO$–$9\%P_2O_5$–$x\%TiO_2$) with compositions of $x = 0$, 1, 2, and 3 mol% (hereafter termed as SCPT0, SCPT1, SCPT2, and SCPT3) of TiO_2 were prepared by sol–gel method [20, 21]. Initially, TEOS, distilled water, and 2M HNO_3 were dissolved in ethanol and then stirred at room temperature for 30 min. After the complete hydrolysis of TEOS, TEP was dissolved into the prepared acidic silica solution and stirred for 20 min. Thereafter, calcium nitrate was dissolved with 5 ml distilled water in a separate container and then dropwise added to the prepared solution followed by addition of titanium isopropoxide. Ammonia solution (1M) was added to the solution until the formation of a gel; that is, until the solution reaches its pH $\sim$8.0. Then, the resulting gel was kept for 48 h in an oven at 60 °C and further dried at 120 °C for 48 h. The obtained powder was ground and calcined at 500 °C for 4 h to remove the carbon and nitrate impurities [22, 23].

Characterization of prepared mesoporous nanobioactive glass particles

X-ray diffraction

The crystalline nature of mesoporous TiO_2-doped NBG particles and HAp layer formation on the glass surface after in vitro studies were characterized by X-ray diffraction (XRD) analysis using an X-ray diffractometer (X'Pert PRO; PANalytical, Almelo, the Netherlands) with Cu Kα as the radiation ($\lambda = 1.5418$ Å) source. The source was operated at 40 kV with 2θ value varying from 10° to 80°.

Fourier transform infrared spectroscopy

The infrared absorption spectra of mesoporous TiO_2-doped NBG particles were measured at room temperature in the

wavenumber range from 4000 to 400 cm^{-1} using a Fourier transform infrared (FTIR) spectrometer (Spectrum 100; PerkinElmer, Shelton, CT, USA). The prepared samples (2 mg each) were mixed with 200 mg KBr in an agate mortar and then pressed into a pellet. For each sample, the FTIR spectrum was normalized with a blank KBr pellet. These measurements were carried out for the prepared glass compositions before and after in vitro studies.

Electron microscopy

Particle size and morphology of the prepared mesoporous NBG particles were determined using images obtained from transmission electron microscopy (TEM; CM 200; Philips, Hillsboro, USA). The surface morphology and elements present in the prepared samples were analyzed using a scanning electron microscope coupled with energy-dispersive X-ray spectrometer (SEM-EDAX; JSM 6360; JEOL, Tokyo, Japan).

X-ray fluorescence spectrometry

Elemental compositions of the prepared mesoporous NBG particles were ascertained using an X-ray fluorescence (XRF) spectrometer (EDX-720; Shimadzu, Kyoto, Japan) to explore the weight loss of the prepared materials during synthesis and also to confirm the apatite formation after in vitro studies.

Surface area analysis

The specific surface area (SSA) of the prepared mesoporous NBG particles was measured using a Barrett–Emmett–Teller (BET) [24] surface area/pore size analyzer (Autosorb AS-1MP; Quantachrome, Boynton Beach, FL). The sample was degassed for 3 h at 295 °C and physisorption analysis was performed with N_2 adsorption measurements at liquid N_2 temperature (−196 °C). Three-point BET was performed to evaluate the pore diameter, pore volume, and SSA of the TiO_2-doped NBG particles. Pore size distribution of the TiO_2-doped NBG particles was evaluated through 10-point adsorption and desorption isotherm using Barrett–Joyner–Halenda method.

In vitro bioactivity

In vitro bioactivity of the prepared mesoporous NBG particles was assessed using acellular, protein-free SBF to evaluate the formation of HAp layer on the surface of the glass. This study was carried out using the standard method proposed by Kokubo and Takadama [25] where the pH value was 7.4 (i.e., equivalent to human blood plasma). The prepared NBG particles (300 mg) were added separately into a polyurethane bottle containing 50 ml SBF and incubated at 37 °C for 21 days. The changes in the pH value of the SBF were measured every day over a period of 21 days using a pH electrode (Orion 720A; 3 Star; Thermo Scientific, Beverly, MA, USA). After 21 days of incubation, the immersed samples were removed from SBF and then gently washed with distilled water and allowed to dry in an oven for 2 h. The dried powders were used for further characterization studies such as XRD, FTIR, SEM, and XRF analyses to reveal the formation of HAp layer on the surface of the glass samples. The weight loss percentage of each sample was calculated using the following equation:

$$\text{Weight loss } \% = (M_0 - M_t/M_0) \times 100 \quad (1)$$

where M_0 is the initial weight of the sample and M_t the weight of the sample measured at time t after being dried.

Antimicrobial study

Antimicrobial properties of the mesoporous NBG particles were tested against clinical pathogens such as *S. aureus* and *E. coli* using Kirby–Bauer disk diffusion method [26]. Mueller–Hinton agar (MHA) medium (HiMedia) was prepared and sterilized at 121 °C (15 psi) for 15 min. The MHA plates were prepared by pouring 15 ml molten medium into sterile Petri plates. The plates were allowed to solidify for approximately 5 min, and 0.1 % of inoculum was swabbed uniformly over the agar until the inoculum became invisible. The NBG-particle-loaded disks, with 10-mm diameter and 2-mm thickness, were placed on culture plates. These plates were incubated overnight at 37 °C. After the incubation period, the diameter of any inhibition zone formed around the cement disk was measured. The above experiments were repeated in triplicates to confirm the homogeneity of the composites.

Cytotoxicity studies

The obtained human osteoblast cell line (MG-63; National Centre for Cell Science, Pune, India) was grown in Eagle's minimum essential medium containing 10 % fetal bovine serum (FBS). The cells were maintained at 37 °C, 5 % CO_2, 95 % air, and 100 % relative humidity. Maintenance cultures were passaged weekly, and the culture medium was changed twice a week.

Cell treatment

The monolayer cells were detached with trypsin–EDTA and viable cells were counted using a hemocytometer and diluted with medium containing 5 % FBS to give final density of 1×10^5 cells per ml. The cell suspension (100 µl/well) was seeded into 96-well plates at a density of

10,000 cells per well. Then, the cells were incubated for cell attachment at 37 °C, 5 % CO_2, 95 % air, and 100 % relative humidity. After 24 h, the cells were treated with the test samples at different concentrations. Additional four serial dilutions were made to provide a total of five sample concentrations. Following sample addition, the plates were incubated for an additional 48 h at the same culture conditions. The medium without samples served as control, and all measurements were undertaken in triplicate.

MTT assay

3-[4,5-Dimethylthiazol-2-yl]2,5-diphenyltetrazolium bromide (MTT) salt cleaved by the mitochondrial enzyme succinate dehydrogenase was used to determine the number of viable cells in the treated wells. After 48 h of cell incubation, 15 µl MTT (5 mg ml^{-1}) in phosphate-buffered saline was added to each well and incubated at 37 °C for 4 h. The medium with MTT was then decanted and formed formazan crystals, which were solubilized in 100 µl dimethyl sulfoxide. The absorbance was measured at 570 nm using a microplate reader. The percentage cell viability then obtained on comparisons with control is as follows:

$$\% \text{ Cell viability} = \frac{\text{Absorbance of the NBG} - \text{treated cells}}{\text{Absorbance of the cells}} \times 100. \quad (2)$$

Results and discussion

The XRD pattern of the prepared base glass and mesoporous TiO_2-doped NBG particles before in vitro studies is shown in Fig. 1. The broad diffraction peaks obtained at diffraction angle (2θ) of 20°–30° show amorphous nature. The addition of TiO_2 in the NBG system does not exert any structural changes while calcinating the prepared samples at 500 °C. Figure 2 shows FTIR spectra of the prepared NBG particles before immersion in the SBF. The peaks observed at 467 and 486 cm^{-1} are assigned to Si–O–Si stretching, whereas those at 794 and 1094 cm^{-1} correspond to symmetric and asymmetric stretching vibrations of Si–O–Si bridging oxygen (Table 1). The bands detected at 636 cm^{-1} correspond to the P=O bond present in the NBG particles. Similarly, the bands detected at 1383 and 1641 cm^{-1} correspond to the hydroxyl group (OH^-) on the glass system. It is inferred from the FTIR analysis that the increase in the concentration of TiO_2 in the NBG system does not result in any major variations.

TEM analysis and selected area electron diffraction (SAED) patterns of the synthesized mesoporous TiO_2-free and TiO_2-doped NBG particles are given in Fig. 3. SCPT1 sample shows a particle size of less than 50 nm with well-dispersed and spherical morphology (Fig. 3b). SCPT0, SCPT2, and SCPT3 glass particles are found to have an irregular spherical morphology and agglomerated particles, as shown in Fig. 3a–d. However, the non-crystalline nature of the prepared TiO_2-doped NBG is evident from the

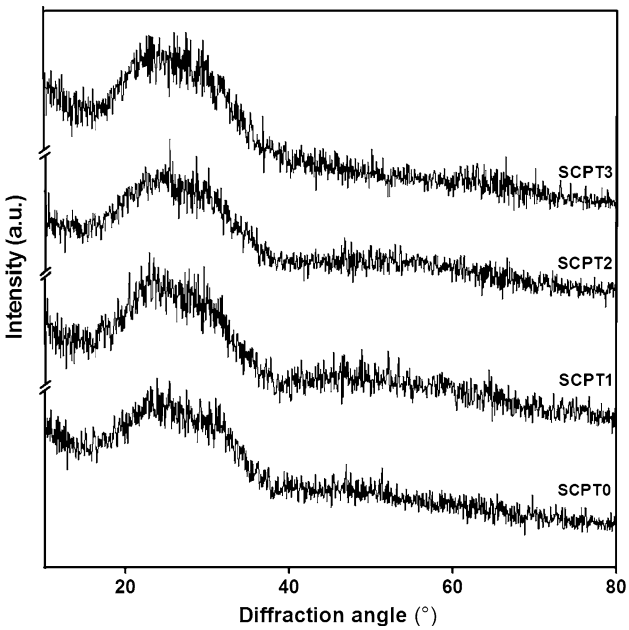

Fig. 1 Diffraction pattern of the as-prepared NBG particles

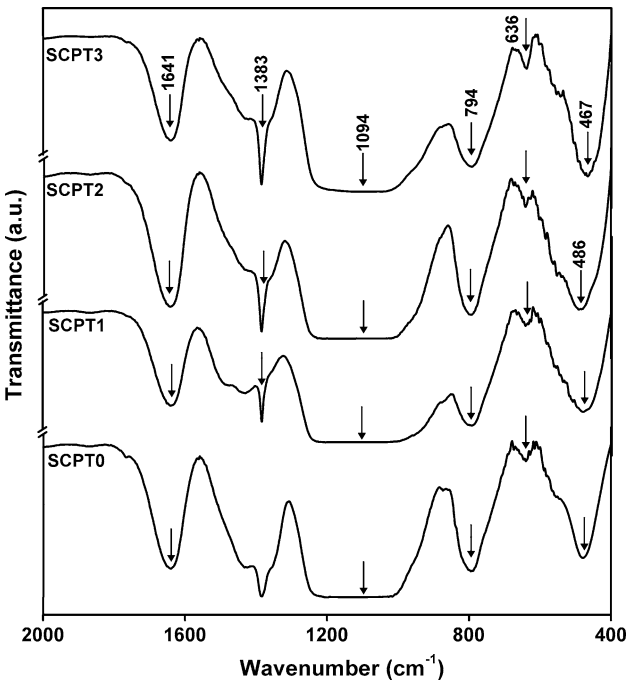

Fig. 2 FTIR spectra of the as-prepared NBG particles

Table 1 Assignments of IR absorption bands in the spectra of before and after in vitro studies of NBG composites

Wavenumber (cm^{-1})								Peak assignments	References
Before in vitro				After in vitro					
SCPT0	SCPT1	SCPT2	SCPT3	SCPT0	SCPT1	SCPT2	SCPT3		
486	486	486	467	–	–	–		Si–O–Si stretching	[37]
–	–	–	–	563	563	563	563	PO_3^{-2} vibration band	[38]
636	636	636	636	598	598	598	–	–P=O bending band, PO_4^{-3} vibration band	[38]
794	794	794		803	803	803	–	Symmetric Si–O–Si stretching in SiO_4 tetrahedron	[37]
–	–	–		873	873	–	873	C–O stretching vibration band in CO_3^{2-}	[37]
1094	1094	1094	1094	1093	1093	1093	1093	Asymmetric Si–O–Si stretching in SiO_4 tetrahedron	[37, 39]
1383	1383	1383	1383	–	–	–		O–H bending vibration band	[40]
–	–	–		1401	1401	1401	1401	C–O stretching vibration band in CO_3^{2-}	[40]
–	–	–		1438	1438	1438	1438	C–O stretching vibration band in CO_3^{2-}	[40]
1641	1641	1641	1641	1644	1644	1644	1530	O–H bending (molecular water)	[40]

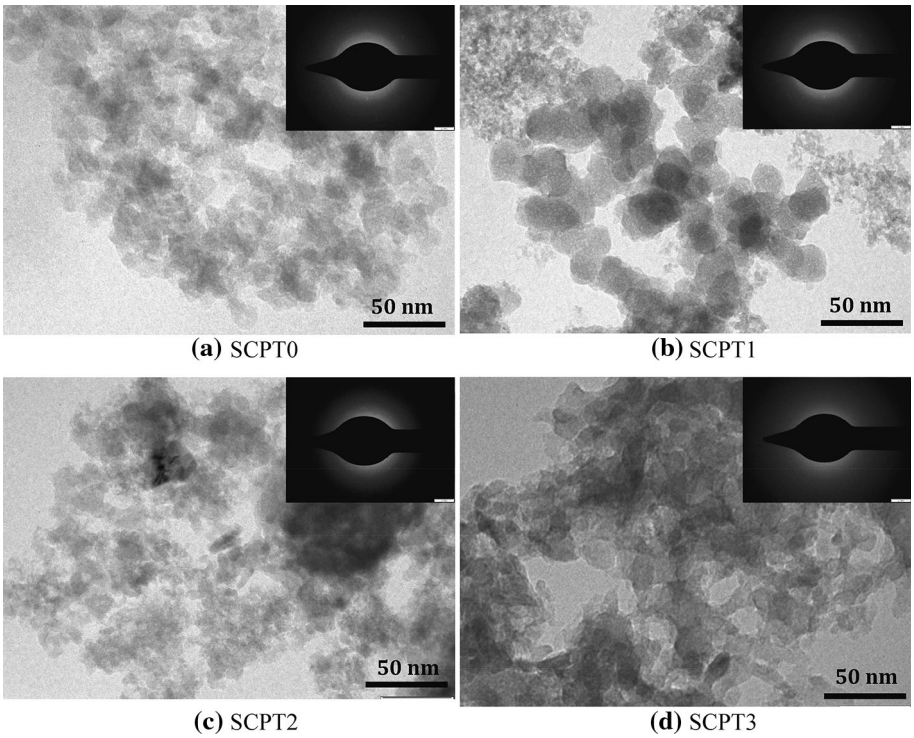

(a) SCPT0 **(b)** SCPT1

(c) SCPT2 **(d)** SCPT3

Fig. 3 TEM images and corresponding diffraction pattern of the NBG particles

SAED pattern (inset in Fig. 3). These results are in good agreement with the XRD results. The observed morphological changes in TiO_2-doped glass systems are due to interchange of Ti ions with Ca^{2+}, which exerts structural changes [12] by acting as an intermediate.

Figure 4 shows the SEM images along with corresponding EDX pattern of the prepared mesoporous NBG particles with different concentrations of TiO_2. From the observed results, it is evident that SCPT0 and SCPT1 samples have spherical shape with uniform morphology whereas samples SCPT2 and SCPT3 have an irregular shape and the particles are agglomerated because of the addition of TiO_2 ($\geq$1 mol%). In addition, the corresponding EDX pattern reveals the elemental compositions of NBG particles with 100 % purity.

The SSA values, pore volume, and average pore diameter of the prepared mesoporous NBG particles are reported in Table 2. The SSA values of SCPT0, SCPT1, SCPT2, and SCPT3 samples are 129, 186, 105, and 129 m^2g^{-1}, respectively. SCPT1 (1 mol% Ti) reveals high

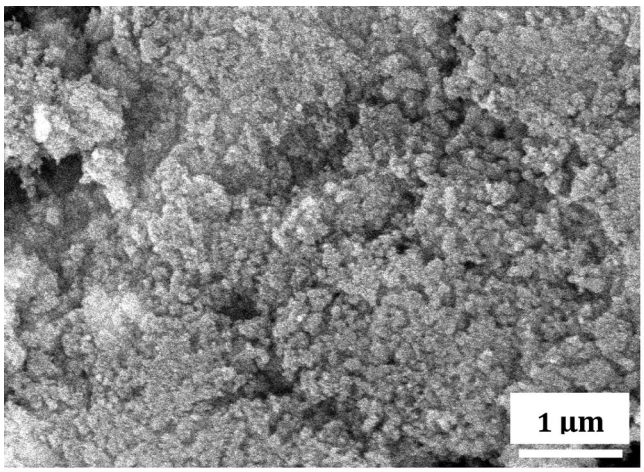

i) SEM image

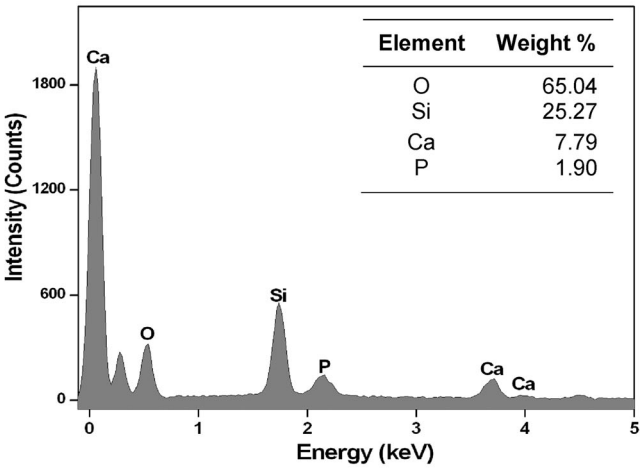

ii) EDX pattern

(a) SCPT0

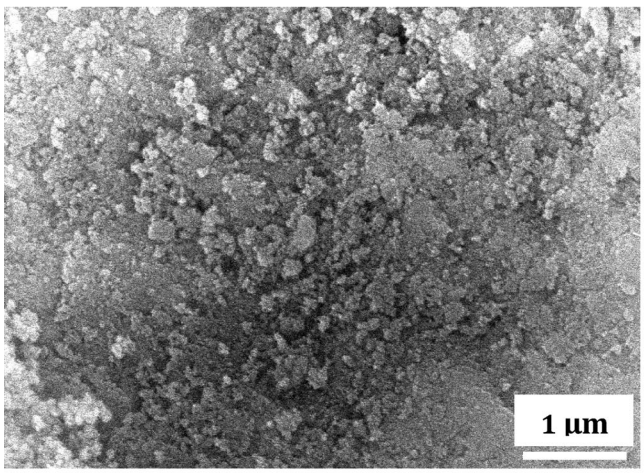

i) SEM image

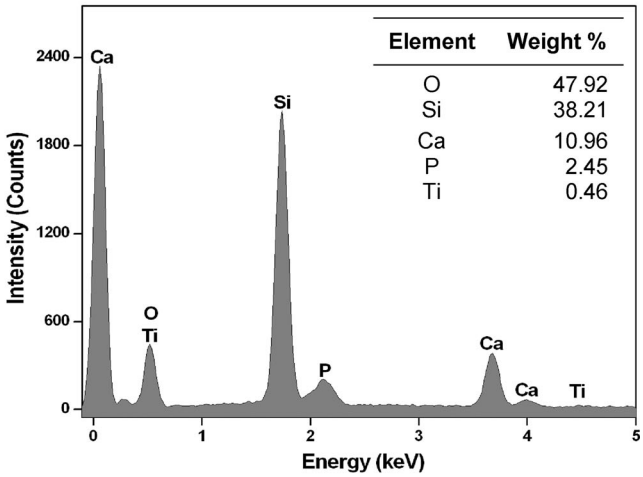

ii) EDX pattern

(b) SCPT1

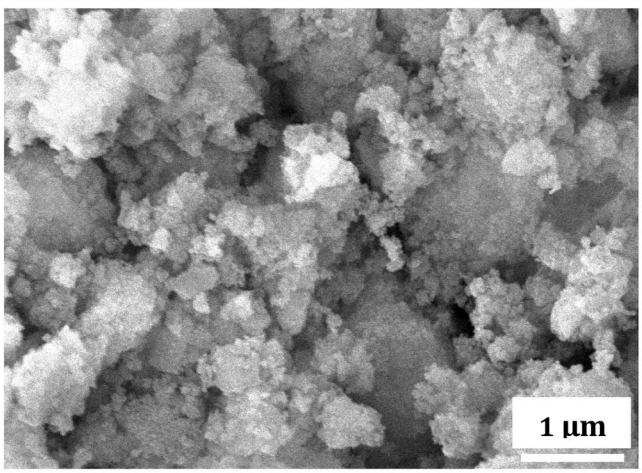

i) SEM image

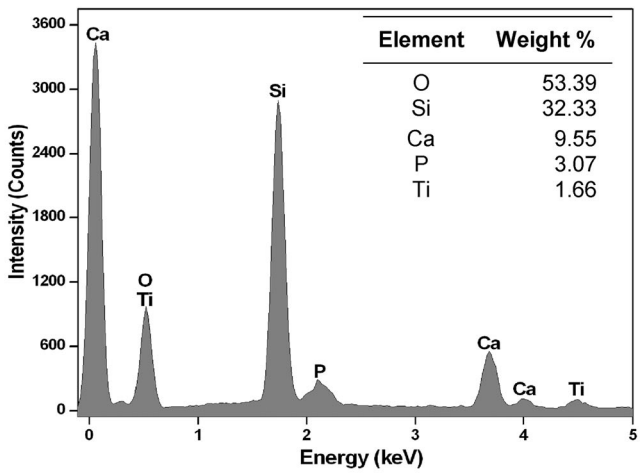

ii) EDX pattern

(c) SCPT2

Fig. 4 SEM images with corresponding EDX pattern of the NBG particles

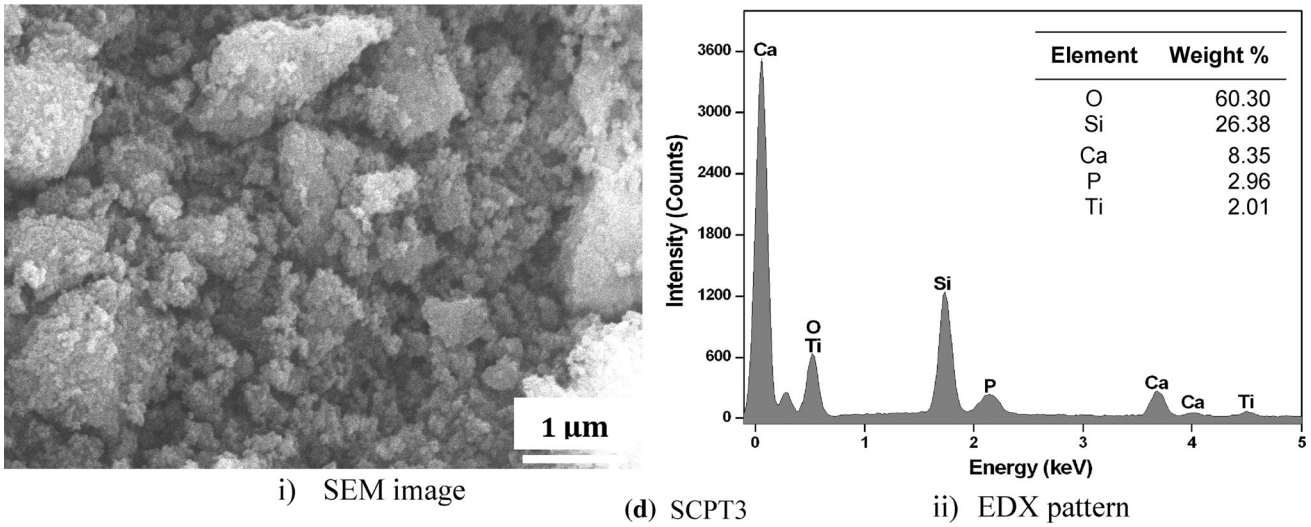

Fig. 4 continued

Table 2 Textural properties and antimicrobial properties of TiO_2-doped NBG glass compositions

Sample code	Surface area (m^2g^{-1})	Average pore diameter (nm)	Total pore volume (cm^3g^{-1})	Zone of inhibition	
				E. Coli (mm)	*S. aureus* (mm)
SCPT0	129	33	1.07	0	0
SCPT1	186	18	0.87	16	0
SCPT2	105	27	0.71	18	0
SCPT3	129	25	0.81	20	0

surface area (186 m^2g^{-1}) when compared with SCPT0 (0 mol% Ti). Further, when the addition of Ti in the NBG is more than 1 mol%, the SSA gradually decreases from 186 m^2g^{-1} (SCPT1) to 105 m^2g^{-1} (SCPT2). However, the SSA of 3 mol% of TiO_2-doped NBG is increased from 105 m^2g^{-1} (SCPT2) to 129 m^2g^{-1} (SCPT3). The total pore volume of the Ti-doped NBG particles is 1.07, 0.87, 0.71, and 0.81 cm^3g^{-1}, respectively, for SCPT0, SCPT1, SCPT2, and SCPT3 samples. Similarly, the average pore diameters of SCPT0, SCPT1, SCPT2, and SCPT3 samples are 33, 18, 27, and 25 nm, respectively. From the observed results, it is evident that the total pore diameter decreases from 33 nm (SCPT0) to 18 nm (SCPT1) while increasing the TiO_2 content from 0 to 1 mol%.

The nitrogen adsorption and desorption isotherm of the mesoporous TiO_2-doped NBG particles is shown in Fig. 5. The observed results show that the prepared NBG particles are extremely mesoporous (<50 nm). The shape of the nitrogen adsorption and desorption isotherm represents a type IIb pattern with a H3 hysteresis loop, which is associated with non-rigid slit-shape pores according to the International Union of Pure and Applied Chemistry (IUPAC) classification [27]. Previous studies show that high surface area of silica- and phosphate-based NBG particles may enhance in vitro bioactivity and biocompatibility, which coincides with the present observation in TiO_2-doped NBG [5, 28].

The prepared Ti-doped NBG glass series are tested for in vitro bioactivity in terms of ionic interaction with SBF. Samples incubated in SBF are regularly monitored for pH variations (Fig. 6). A sudden increase in pH value is observed in the Ti-doped NBG particles immersed in SBF up to day 3, which may be due to the effect of Ti ions on the base glass. Addition of titania to glass initially causes a rise in pH during initial ion release and later it forms phosphoric acid by absorbing phosphate ions into the solution, which causes a decrease in pH [13]. After day 6, the SBF shows a decrease in the pH value of all the NBG particles due to gradual increase in the absorption of Ca^{2+} and P^{5+} ions from the SBF to induce the formation of HAp layer on the surface of NBG particles. However, there is no significant variation in any sample after 15 days. However, SCPT1 sample remains constant in pH from 15 to 21 days, which may be due to saturation of ion exchange after formation of HAp layer in SBF. After 21 days of immersion in SBF, the NBG particles are dried and characterized by XRD, FTIR, and SEM studies.

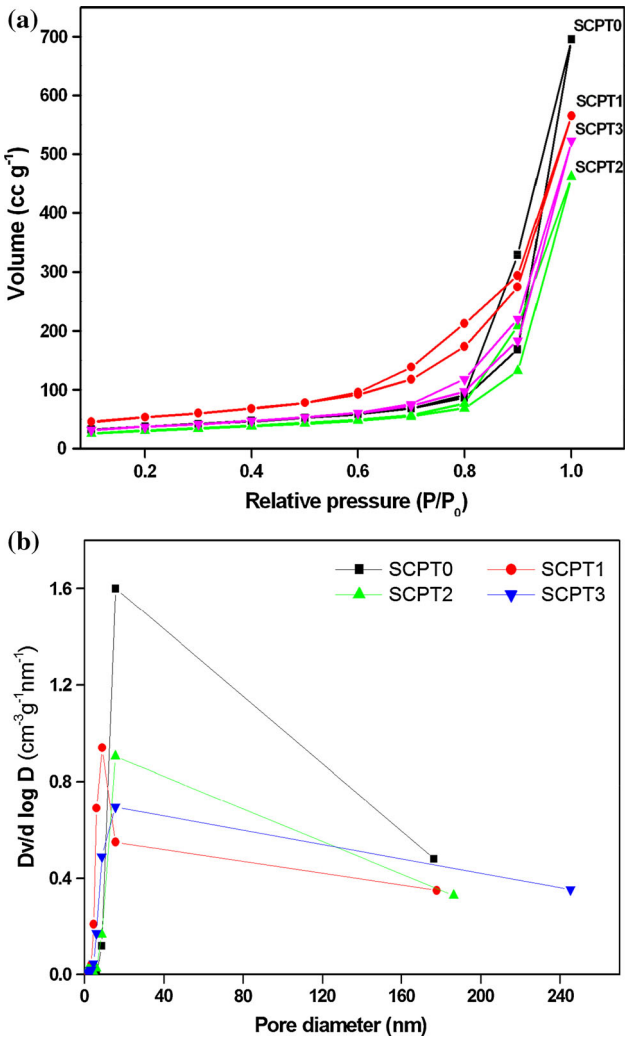

Fig. 5 The N_2 adsorption and desorption isotherms of prepared the NBG particles

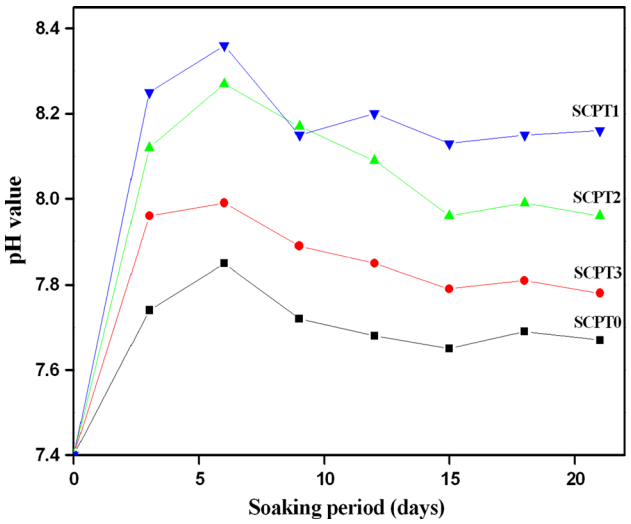

Fig. 6 pH variation during different immersion periods for the NBG samples

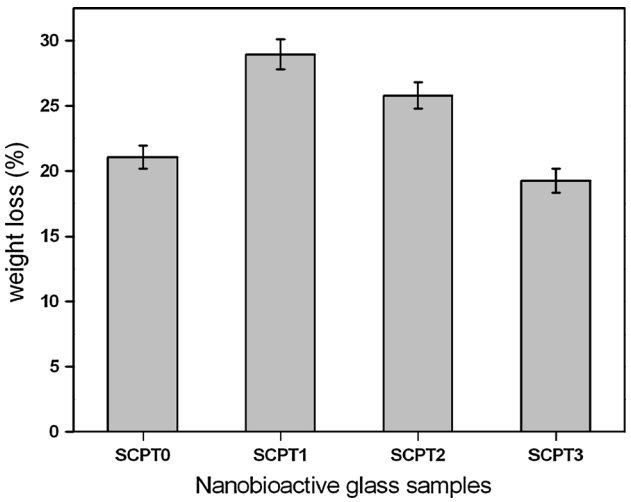

Fig. 7 Degradation percentage of the prepared NBG particles after 21 days of immersion in SBF

The weight loss percentage of mesoporous NBG particles in the SBF is shown in Fig. 7. It is observed that the weight loss percentage of TiO_2-doped NBG increases as the concentration of TiO_2 increases up to 1 %. The degradation rates of the NBG particles are 21.05, 28.95, 25.79, and 19.26 %, respectively, for SCPT0, SCPT1, SCPT2, and SCPT3 samples. The TiO_2-free NBG sample (SCPT0) shows a decrease in the weight loss as compared to TiO_2-doped glasses. However, substitution of TiO_2 (1 mol%) for CaO increases the degradability of glass particles and improves apatite formation on the glass surface (SCPT1). The increase in TiO_2 ($\geq$1 %) decreases the degradation rate because of low dissolution rate of SCPT2 and SCPT3 samples. It may delay apatite formation on the glass surface and solubility of the glass. It is evident from the earlier studies that the presence of Ti in the phosphate network acts as both the network former and network modifier [29, 30]. The observed decrease in weight loss may be due to the breaking of P–O–P bonds in phosphate network structure, leading to formation of terminal oxygens. Similarly, the reinforcement of glass structure might have taken place due to creation of non-bridging oxygen of two phosphate chains when the concentration of TiO_2 is less than 1 %. Thus, it may lead to decrease in degradation of glass particles. Therefore, the degradation rate of the NBG particles changes depending on the concentration of TiO_2.

Figure 8 shows the XRD pattern of the mesoporous NBG particles after 21 days of immersion in SBF. The observed diffraction crystalline peaks in SCPT0 and SCPT1 samples at 28.9°, 31.7°, and 31.9° (JCPDS file no.

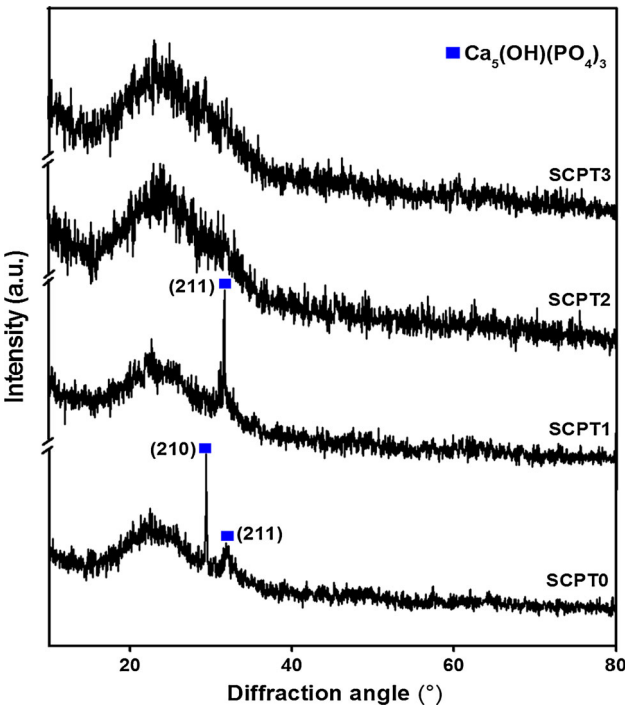

Fig. 8 XRD pattern of the NBG particles after 21 days of immersion in SBF

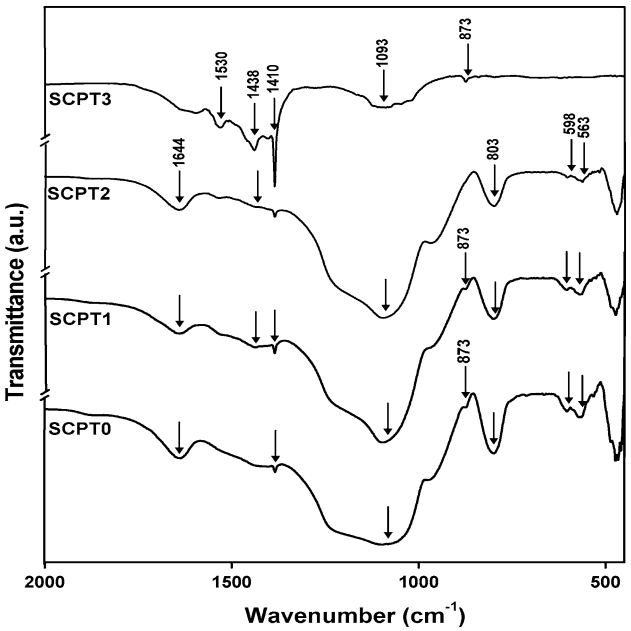

Fig. 9 FTIR spectra of NBG particles after immersion in SBF for 21 days

09-0432) correspond to the formation of HAp layer on the glass surface. The observed results distinctly indicate that the rate of HAp layer formation is high in SCPT1 compared with that in SCPT0, SCPT2, and SCPT3 samples. SCPT2 and SCPT3 samples reveal amorphous nature, which may be due to low dissolution rate of NBG particles in SBF. When the concentration of Ti increases above 1 %, it suppresses the dissolution rate and reduces the rate of HAp layer formation. In addition, higher concentration of amorphous TiO_2 does not induce apatite formation on its surface in SBF [31].

The formation of HAp layer on the surface of the mesoporous NBG particles after SBF incubation is examined from the obtained FTIR spectra (Fig. 9). The peaks observed at 598 and 563 cm^{-1} correspond to the absorption of the phosphate band, which confirms HAp layer formation on the surface. In addition, the absorption of carbonate peaks at 1438, 1401, and 873 cm^{-1} are also detected in SCPT1 sample. The peaks observed at 803 and 1093 cm^{-1} indicate Si–O–Si asymmetric stretching vibration and the peak observed at 1644 cm^{-1} indicates the presence of hydroxyl group (Table 1). However, it is resolved that the development of carbonate band is higher in SCPT1 than that in SCPT2 and SCPT3. The well-developed carbonate and phosphate bands indicate the formation of HAp layer on the NBG surface. In addition, the suppressed or delayed HAp layer formation in 2 and 3 mol% Ti-doped NBG particles is due to low dissolution or degradation of Ca^{2+} and P^{5+} ions in SBF [32].

The SEM images of mesoporous NBG particles (SCPT0, SCPT1, SCPT2, and SCPT3) obtained after immersion in SBF for 21 days are depicted in Fig. 10a–d. The morphological difference is observed only in SCPT1 sample before and after immersion in SBF, indicating the formation of new apatite crystals on the surface. SCPT0, SCPT2, and SCPT3 samples show less formation of HAp layer on the glass surface after in vitro studies. Formation of HAp crystal is clearly visible on the surface of SCPT1 sample (Fig. 10b) when compared with other TiO_2-doped NBG particles. The above results show that reactivity of 1 mol% TiO_2-doped NBG particles with SBF is high, and hence, the glass surface is fully covered with a crystalline HAp layer without any interface. As the concentration of Ti increases above 1 %, it changes the structure and reduces the dissolution rate of the NBG particles [14].

The in vitro bioactivity via formation of HAp layer on the surface of mesoporous NBG particles is confirmed by XRF analysis. The elemental composition with weight percentage of Ti-doped NBG particles before and after SBF immersions is given in Table 3. From the observed results, it is clear that the formation of CaP surface layer increases whereas the amount of Si content decreases on the sample surface after immersion in SBF for 21 days. In addition, SCPT1 sample shows Ca/P ratio of 1.74, which is closer to the appropriate stoichiometric value (1.67) of HAp. On the basis of the XRD, FTIR, and SEM results, it is concluded that SCPT1 shows better in vitro bioactivity

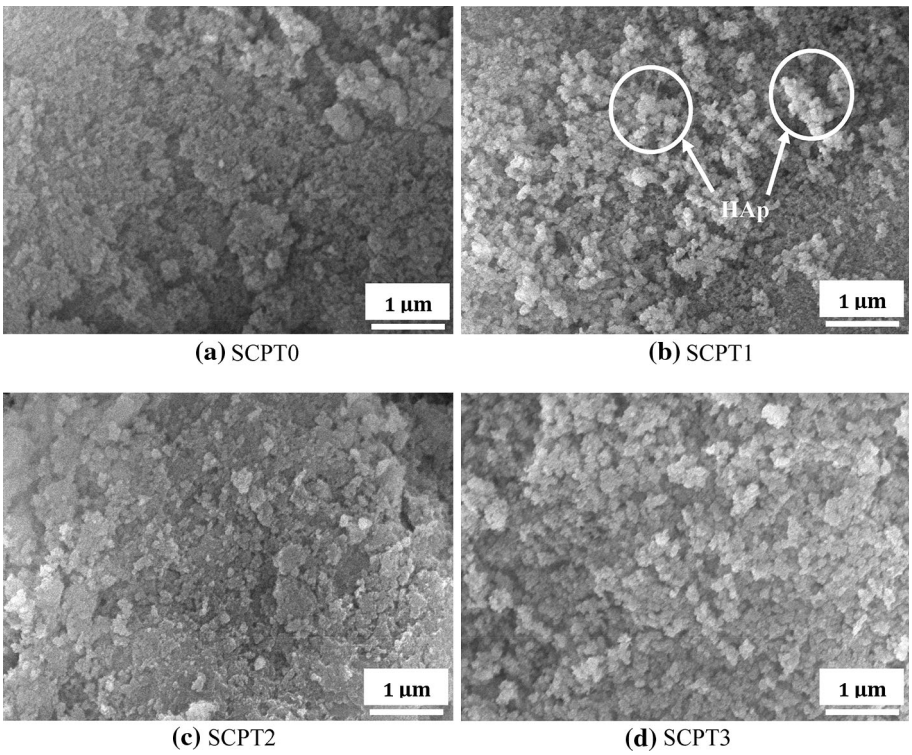

Fig. 10 SEM images of different NBG particles after incubation in SBF for 21 days

(a) SCPT0 **(b)** SCPT1 **(c)** SCPT2 **(d)** SCPT3

Table 3 XRF analysis of TiO_2-doped NBG particles before and after in vitro

	Before immersion (wt %)			After immersion (wt%)			
Sample	Si	Ca	P	Si	Ca	P	Ca/P
SCPT0	32.35	9.75	4.65	28.69	11.87	08.60	1.38
SCPT1	40.24	12.62	6.72	35.62	16.31	9.34	1.74
SCPT2	34.83	11.56	5.98	32.14	11.48	04.70	2.44
SCPT3	31.49	10.09	7.82	30.45	09.63	3.65	2.63

and biocompatibility with respect to SSA when compared with SCPT2 and SCPT3.

The response of bacteria to the prepared mesoporous Ti-doped NBG particles is tested against *S. aureus* and *E. coli*, as shown in Fig. 11. No zone of inhibition is observed against *S. aureus* for all the prepared NBG particles, whereas it is found that the concentration of Ti increases the zone of inhibition against *E. coli* (Table 2). The measured inhibition zone in *E. coli* placed with SCPT1, SCPT2, and SCPT3 sample is 16, 18, and 20 mm, respectively. It is shown that the bactericidal activity of TiO_2-doped NBG particles is induced by the oxidizing reaction of reactive oxygen species [19]. However, TiO_2-doped NBG particles show no significant microbial activity due to least contact between *S. aureus* and the prepared amorphous NBG particles [19]. Therefore, it is evident that TiO_2 nanoparticles induce a huge amount of hydroxyl radicals [18] against gram-negative bacteria, which leads to a greater antibacterial activity against *E. coli*.

The in vitro cell viability and cytotoxicity assays are performed for mesoporous NBG glass composites against osteoblast cell line (MG-63). NBG-particle-treated osteoblast cells at different concentrations (31.25, 62.5, 125, 250, and 500 µg ml^{-1}) are observed microscopically (images not shown) for cell mobility and cell death. The observed results revealed that SCPT0 and SCPT1 samples did not show any cell damage at 31.25, 62.5, and 125 µg ml^{-1} concentrations when compared with SCPT2 and SCPT3 samples. However, cell damage is observed when the concentration reaches above 62.5 µg ml^{-1} for SCPT2 and SCPT3 samples.

The cell viability percentage of the mesoporous NBG particles at different concentrations is determined by MTT assay. The obtained cell viability percentage is given in histogram (Fig. 12). After 48 h of incubation, the cell viability percentages at a concentration of 31.25, 62.5, 125, 250, and 500 µg ml^{-1} are 103, 101, 98, 84, and 78 % for SCPT1 samples. This indicates that SCPT1 sample is non-toxic at a concentration up to 125 µg ml^{-1}. A significant decrease in cell viability is observed in SCPT2 and SCPT3 samples (Fig. 12) when compared with SCPT0 and SCPT1 samples. NBG doped with 1 % TiO_2 is the optimal composition for the formation of HAp layer and better biocompatibility due to release of ions essential for cell

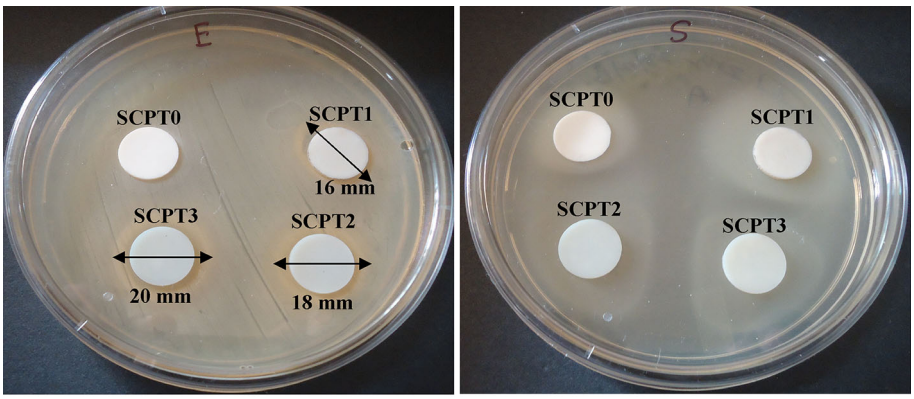

Fig. 11 Antimicrobial activity of NBG particles against *E. coli* and *S. aureus*

(a) *Escherichia coli* **(b)** *Staphylococcus aureus*

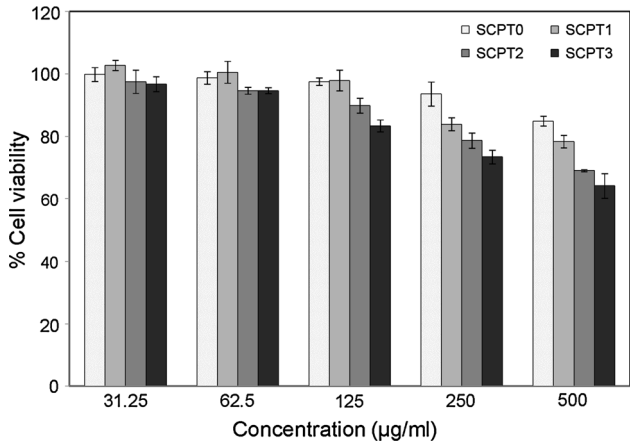

Fig. 12 In vitro biocompatibility of NBG particles by MTT assay in osteoblast cell line (MG-63)

attachment. The cell viability and HAp layer formation are found to be low in SCPT2 and SCPT3 because of low dissolubility of glass sample, which leads to an unfavorable environment for cell attachment and proliferation [33]. As the concentration of titanium increases above 1 % in the NBG sample, the cell viability decreases, exerting toxic effects on cells.

The toxicity of mesoporous NBG particles depends not only on the concentration but also on size, shape, and physicochemical stability of the particles [34]. However, when the concentration of Ti-doped NBG particles increases above 125 µg ml^{-1}, it may induce phenotypic changes due to release of cytokines and proteases in the cells. It might result in reduced bone formation due to the effect of osteoblast differentiation, osteoblast recruitment, and matrix formation [35, 36]. Therefore, SCPT1 sample shows better bioactivity and higher cytocompatibility against osteoblast cells than control and could basically serve as an effective material for biomedical implant applications.

Conclusion

TiO_2-free and TiO_2-doped mesoporous NBG particles were synthesized by simple and cost-effective sol–gel method. The physicochemical properties of these nanoparticles were characterized to optimize glass compositions for enhanced in vitro bioactivity, antimicrobial activity, and biocompatibility. The results of this investigation show that SCPT1 reveals uniform spherical morphology and higher SSA of 186 m^2g^{-1} with amorphous nature. The formation of the HAp layer on the sample surface was confirmed by SEM–EDS, XRD, and XRF analyses. Higher antimicrobial activity of the prepared TiO_2-doped NBG particles was observed against *E. coli*, whereas no significant response was observed against *S. aureus*. The addition of TiO_2 (1 mol%) in glass compositions showed nontoxic effect and exhibited better cell viability in osteoblast cell line (MG-63) at a concentration of 125 µg ml^{-1}. From the observed results, it is concluded that TiO_2-doped NBG particles (1 mol%) could be treated as a possible NBG composite for medical implant applications with better bioactivity and biocompatibility.

Acknowledgements The authors acknowledge the financial support (SR/S2/CMP-0054/2009 dt. 27.09.2010) provided by the Department of Science and Technology (DST), New Delhi, to carry out this research project.

References

1. Abou Neel EA, Chrzanowski W, Valappil SP, O'Dell LA, Pickup DM, Smith ME, Newport RJ, Knowles JC (2009) Doping of a high calcium oxide metaphosphate glass with titanium dioxide. J Non Cryst Solids 355:991–1000
2. Prabhu M, Kavitha K, Manivasakan P, Rajendran V, Kulandaivelu P (2013) Synthesis, characterization and biological response of magnesium substituted nanobioactive glass particles for biomedical applications. Ceram Int 39:1683–1694
3. Jones JR (2013) Review of bioactive glass: from Hench to hybrids. Acta Biomater 9:4457–4486

4. Hench LL, Thompson I (2010) Twenty-first century challenges for biomaterials. J R Soc Interface 7:S379–S391
5. Prabhu M, Kavitha K, Suriyaprabha R et al (2013) Preparation and characterization of silver-doped nanobioactive glass particles and their in vitro behaviour for biomedical applications. J Nanosci Nanotech 13:5327–5339
6. Li Z, Qu Y, Zhang X, Yang B (2009) Bioactive nano-titania ceramics with biomechanical compatibility prepared by doping with piezoelectric $BaTiO_3$. Acta Biomater 5:2189–2195
7. Kavitha K, Sutha S, Prabhu M, Rajendran V, Jayakumar T (2013) In situ synthesized novel biocompatible titania-chitosan nanocomposites with high surface area and antibacterial activity. Carbohydr Polym 93:731–739
8. Shah Mohammadi M, Chicatun F, Stähli C, Muja N, Bureau MN, Nazhat SN (2014) Osteoblastic differentiation under controlled bioactive ion release by silica and titania doped sodium-free calcium phosphate-based glass. Colloids Surf B 121:82–91
9. Dhayal M, Kapoor R, Sistla PG, Pandey RR, Kar S, Saini KK, Pande G (2014) Strategies to prepare TiO_2 thin films, doped with transition metal ions, that exhibit specific physicochemical properties to support osteoblast cell adhesion and proliferation. Mater Sci Eng C 37:99–107
10. Shahadat M, Teng TT, Rafatullah M, Arshad M (2015) Titanium-based nanocomposite materials: a review of recent advances and perspectives. Colloids Surf B 126C:121–137
11. Kavitha K, Prabhu M, Rajendran V, Manivasankan P, Prabu P, Jayakumar T (2013) Optimization of nano-titania and titania-chitosan nanocomposite to enhance biocompatibility. Curr Nanosci 9:308–317
12. Martin RA, Moss RM, Lakhkar NJ, Knowles JC, Cuello GJ, Smith ME, Hanna JV, Newport RJ (2012) Structural characterization of titanium-doped Bioglass using isotopic substitution neutron diffraction. Phys Chem Chem Phys 14(45):15807–15815
13. Lakhkar NJ, Park JH, Mordan NJ, Salih V, Wall IB, Kim HW, King SP, Hanna JV, Martin RA, Addison O, Mosselmans JF, Knowles JC (2012) Titanium phosphate glass microspheres for bone tissue engineering. Acta Biomater 8(11):4181–4190
14. Asif IM, Shelton RM, Cooper PR, Addison O, Martin RA (2014) In vitro bioactivity of titanium-doped bioglass. J Mater Sci Mater Med 25(8):1865–1873
15. Monem AS, ElBatal HA, Khalil EMA, Azooz MA, Hamdy YM (2008) In vivo behavior of bioactive phosphate glass-ceramics from the system P_2O_5-Na_2O-CaO containing TiO_2. J Mater Sci Mater Med 19:1097–1108
16. Nan Y, Lee WE, James PF (1992) Crystallization behavior of CaO-P_2O_5 glass with TiO_2, SiO_2, and Al_2O_3 additions. J Am Ceram Soc 75:1641
17. Chen Q, Miyaji F, Kokubo T, Nakamura T (1999) Apatite formation on PDMS-modified CaO-SiO_2-TiO_2 hybrids prepared by sol-gel process. Biomaterials 20(12):1127–1132
18. Kim YS, Linh LT, Park ES, Chin S, Bae G-N, Jurng J (2012) Antibacterial performance of TiO_2 ultrafine synthesized by a chemical vapor condensation method: effect of synthesis temperature and precursor vapor concentration. Powder Technol 215–216:195–199
19. Caballero L, Whitehead KA, Allen NS, Verran J (2009) Inactivation of *E.coli* on immobilized TiO_2 using fluorescent light. J Photochem Photobiol A 202:92–98
20. Saravanakumar B, Prabhu M, Rajendran V (2013) Electrochemical deposition of $58SiO_2$-$33CaO$-$9P_2O_5$ nanobioactive glass particles on Ti-6Al-4V alloy for biomedical applications. Int J Appl Ceram Technol. doi:10.1111/ijac.12124
21. Bielby RC, Christodoulou IS, Pryce RS, Radford WJP, Hench LL, Polak JM (2004) Time- and concentration-dependent effects of dissolution products of 58S sol-gel bioactive glass on proliferation and differentiation of murine and human osteoblasts. Tissue Eng 10:1018–1026
22. FitzGerald V, Martin RA, Jones JR, Qiu D, Wetherall KM, Moss RM, Newport RJ (2009) Bioactive glass sol-gel foam scaffolds: evolution of nanoporosity during processing and in situ monitoring of apatite layer formation using small- and wide-angle X-ray scattering. J Biomed Mater Res A. 91(1):76–83
23. Yu B, Turdean-Ionescu CA, Martin RA, Newport RJ, Hanna JV, Smith ME, Jones JR (2012) Effect of calcium source on structure and properties of sol-gel derived bioactive glasses. Langmuir 28(50):17465–17476
24. Brunauer S, Emmett PH, Teller E (1938) Adsorption of gases in multimolecular layers. J Am Chem Soc 60:309
25. Kokubo T, Takadama H (2006) How useful is SBF in predicting in vivo bone bioactivity? Biomaterials 27:2907–2915
26. Bauer A, Kirby WMM, Sherris JC, Turch M (1966) Antibiotic susceptibility testing by a standardized single disk method. Am J Clin Pathol 45:493–496
27. Rouquerol F, Rouquerol J, Sing K (1999) Chapter 13—General conclusions and recommendations, adsorption by powders and porous solids. Academic Press, Amsterdam, pp 439–447
28. Yun H-S, Kim S-H, Lee S, Song I-H (2010) Synthesis of high surface area mesoporous bioactive glass nanospheres. Mater Lett 64:1850–1853
29. Rajendran V, Rajkumar G, Aravindan S, Saravanakumar B (2010) Analysis of physical properties and hydroxyapatite precipitation in vitro of TiO_2-containing phosphate-based glass systems. J Am Ceram Soc 93(12):4053
30. Barbieri L, Bonamartini Corradi A, Leonelli C, Siligardi C, Manfredini T, Carlo Pellacani G (1997) Effect of TiO_2 addition on the properties of complex aluminosilicate glasses and glass-ceramics. Mater Res Bull 32(6):637
31. Uchida M, Kim HM, Kokubo T, Fujibayashi S, Nakamura T (2003) Structural dependence of apatite formation on titania gels in a simulated body fluid. J Biomed Mater Res 64a:164
32. Ducheyne P, Radin S, King L (1993) The effect of calcium-phosphate ceramic composition and structure on in vitro behavior. I. Dissoultion. J Biomed Mater Res 27:25–34
33. Ni S, Chang J, Chou L (2008) In vitro studies of novel CaO-SiO_2-MgO system composite bioceramics. J Mater Sci Mater Med 19:359–367
34. Gerhardt L-C, Jell GMR, Boccaccini AR (2007) Titanium dioxide (TiO2) nanoparticles filled polyD, L-lactid acid (PDLLA) matrix composites for bone tissue engineering. J Mater Sci Mater Med 18:1287–1298
35. Savaiano JK, Webster TJ (2004) Altered responses of chondrocytes to nanophase PLGA/nanophase titania composites. Biomaterials 25:1205–1213
36. Wooley PH, Schwarz EM (2004) Aseptic loosening. Gene Ther 11:402–407
37. Talos F, Senila M, Frentiu T, Simon S (2013) Effect of titanium ions on the ion release rate and uptake at the interface of silica based xerogels with simulated body fluid. Corros Sci 72:41–46
38. Pena J, Izquierdo-Barba I, Martinez A, Vallet-Regi M (2006) New method to obtain chitosan/apatite materials at room temperature. Solid State Sci 8:513–519
39. Vasconcelos HC (2010) The effect of PO2, 5 and AlO1, 5 additions on structural changes and crystallization behavior of SiO_2-TiO_2 sol-gel derived glasses and thin films. J Sol Gel Sci Technol 55:126–133
40. Socrates G (2004) Infrared and raman characteristic group frequencies: tables and charts, 3rd edn. Wiley, Chichester